Tertiary Compression Creep of Long-Fiber Composites: A Model for Fiber Kinking and Buckling

T.A. VENKATESH and D.C. DUNAND

The uniaxial compression-creep behavior of unidirectionally reinforced continuous-fiber composite materials was investigated for the case where both the matrix and the fiber underwent plastic deformation by creep. The creep behavior of NiAl composites reinforced with 5 to 20 vol pct tungsten fibers was characterized at 1025 °C. The NiAl-W composites exhibited a three-stage creep behavior, with distinct primary, secondary, and tertiary creep. Microstructurally, tertiary creep was characterized by one of the following fiber-deformation mechanisms: brooming, bulging, buckling, or kinking. The composite tertiary creep is modeled by solving for global or local kink-band evolution, with composite deformation contributing, respectively, to fiber buckling or kinking. The model predicts (1) the critical strain for the onset of the tertiary stage to be most sensitive to the initial kink angles, while being relatively insensitive to the initial kink-band heights and (2) the critical strain to vary inversely with the volume fraction of fiber in the composite. Reasonable agreement between model predictions and experiments is obtained.

I. INTRODUCTION

AMONG metal-matrix composites, unidirectional continuous fiber–reinforced composites exhibit the highest specific strength and stiffness. Their tensile[1] and compressive behavior[2–6] at low temperatures has been studied extensively. The composite response to tensile stresses at elevated temperatures, where creep of the matrix or of both the matrix and reinforcement is the dominant deformation mechanism, has also been modeled successfully.[7] While the compressive response of these composites is expected to be qualitatively similar to their tensile response during the primary and secondary creep stages, the onset and progression of instabilities in compression are expected to be different from those in tension and could pose serious design limitations for composite use at elevated temperatures.[8]

A review of relevant literature indicates that very few compression-creep studies, primarily experimental in nature, have been conducted on metal-matrix composites. First, in the NiAl-Al_20_3 system,[9] more than 10 pct creep strain was accumulated before samples failed by macrobuckling or delamination. While the microstructural effects were not investigated, it is quite likely that extensive fracture of alumina fibers contributed to the tertiary behavior. Second, in the eutectic Al-$CuAl_2$ system,[10] primary, secondary, and tertiary creep behaviors were observed. While microstructural evidence for elastic bending and subsequent buckling of the $CuAl_2$ lamellae was found during the secondary and tertiary creep regimes, respectively, no mechanics modeling was undertaken. Third, in the $MoSi_2$-Nb system,[11] two types of behavior were observed. Below the brittle-to-ductile transition temperature, very low failure strains were obtained as a consequence of matrix cracking. Above the transition temperature, larger strains to failure were observed. No microstructural investigation of the deformed niobium fibers was conducted. It is expected that both the niobium fibers and the $MoSi_2$ matrix would have crept under these test conditions.

As for ceramic-matrix composites, one study[12] investigated creep of a SiC fiber–reinforced carbon composite and concluded that the composite creep was controlled by creep of the SiC fibers as a result of matrix failure by cracking. Very few creep studies exist for polymer matrix composites under compression.[13]

We chose the NiAl-W system as a model system to systematically study the compression-creep behavior of long-fiber composites for the case where both the (NiAl) matrix and the (tungsten) fibers exhibited creep deformation. These composites, in general, displayed three-stage creep behavior with distinct primary, secondary, and tertiary stages.[14–16]

The primary creep of these composites was modeled[15] by considering the primary creep of the individual phases as well as the transient stress states arising from load transfer from the weaker matrix phase to the stronger fiber phase as the composite transitioned from the elastic or elasto-plastic state, present immediately after loading, to the steady-state stage, where both phases deformed by creep. The model predicted, in good agreement with experiments, the composite primary creep strain to be significant at high composite stresses and for high fiber volume fractions and the primary creep time to be uniquely related to the composite steady-state creep rate.

The secondary creep of these composites was microstructurally characterized by uniaxial compression of the tungsten fibers and was predicted[16] reasonably well with a rule-of-mixtures iso-strain model developed for composites where both phases deformed by creep, using compression-creep results of the as-processed (NiAl) matrix and tensile-creep results of the as-received (tungsten) fibers.

While the occurrence of the tertiary stage of creep in the compression-creep experiments was noted in an earlier work,[16] a systematic study of this stage of creep has not

T.A. VENKATESH, Postdoctoral Research Associate, is with the Department of Materials Science and Engineering, Massachusetts Institute of Technology, Cambridge, MA 02139. D.C. DUNAND, Associate Professor, formerly with the Department of Materials Science and Engineering, Massachusetts Institute of Technology, is with the Department of Materials Science and Engineering, Northwestern University, Evanston, IL 60208.

Manuscript submitted December 1, 1999.

been presented thus far. Hence, the objectives of this investigation are, using NiAl-W as a model system, to identify the dominant deformation mechanisms for tertiary creep of unidirectionally reinforced continuous-fiber composites subjected to uniaxial compression at elevated temperatures, to develop simple mechanistic models to characterize their tertiary compressive-creep response for different deformation modes, and to obtain experimental verification of these models.

II. EXPERIMENTS

A. *Materials Selection*

The NiAl-W system was chosen for this investigation for the following four reasons. First, NiAl exhibits low density, high melting point, good oxidation resistance, high thermal conductivity, and a wide range of compositional stability and is, thus, a potential candidate to replace nickel-based superalloys in high-temperature structural applications.[17–19] However, the NiAl system has two major limitations:[20] (1) poor creep strength at elevated temperatures and (2) low ductility and toughness at low temperatures (below the brittle-to-ductile transition temperature). Second, tungsten offers excellent specific creep resistance at high temperatures,[21–23] thus addressing the first limitation of NiAl. Third, the NiAl-W composite system exhibits very good chemical stability, as tungsten is thermodynamically stable with, and has virtually zero solid solubility in, NiAl.[24] NiAl protects tungsten from oxidation, while tungsten enhances toughness through ductile-phase toughening mechanisms at low temperatures, thus addressing the second limitation of NiAl. Finally, reactive infiltration, a novel processing technique that combines the advantages of reactive synthesis with those of infiltration processing, has been developed to process NiAl[16,25] and NiAl-W composites.[16]

B. *Experimental Procedures*

As described in Reference 16, cylindrical billets of NiAl reinforced with 5 to 20 vol pct tungsten wires were fabricated by reactive infiltration. Creep samples 10 and 20 mm in height and with circular and square cross sections 5 mm in diameter and width, respectively, were electrodischarge machined from the billets. The composite samples had fibers aligned with their longitudinal direction.

Constant-load uniaxial compression-creep tests were performed in air on NiAl-W composites (Table I) at 1025 °C within an applied stress range from 80 to 120 MPa, as described in more detail in Reference 16. Frictional effects on the end-loaded samples were minimized by using boron nitride–coated flat alumina platens in the creep cage. Alumina platens with a recess depth of 1 mm were also used in some experiments to prevent sample brooming.

The matrix of as-cast and creep-tested NiA1-W composites was dissolved in aqua-regia (3 HCl:1 HNO_3 by volume) at room temperature for times between 4 and 8 hours. Tungsten fibers were extracted to compare the fiber geometry before and after the test. From a count of the tungsten fibers recovered from each sample, the volume fractions of tungsten in the composite samples were obtained. Pure tungsten fibers exhibited negligible dissolution when treated with aqua-regia.

III. RESULTS

All experiments, with or without flat platens (*i.e.*, the recessed alumina platens) and irrespective of sample aspect ratios, exhibited significant primary creep (discussed in Reference 15), followed by stable secondary creep over varying amounts of strains (discussed in Reference 16) and a subsequent tertiary stage with a rapid increase in strain rates (Figures 1 and 2).

Visual inspection of the as-fabricated and creep-tested samples, coupled with the tungsten fibers extracted from the untested sample (Figure 3(b)) and tested samples, revealed that the tertiary stage was associated with four modes of fiber deformation: (1) brooming (Figure 3(c)), which occurred in samples with an aspect ratio of 2 and tested using a flat platens; (2) bulging (Figure 3(d)), which took place predominantly in samples with an aspect ratio of 2 and tested using recessed platens; (3) buckling (Figure 3(e), which was found only in sample 2; and (4) kinking (Figure 3(f)), which occurred only in samples with an aspect ratio of 4 and tested using recessed platens.

IV. DISCUSSION

The NiAl-W composites loaded uniaxially in compression in the direction of fibers, at temperatures where both the fiber and matrix creep, exhibit a primary-creep transient, as discussed in Reference 15. This primary stage is followed by a secondary creep regime characterized by a steady state in the composite creep rate when both creeping constituents attain their respective steady-state stress, after load partitioning is completed, as discussed in Reference 16. This secondary stage can be followed by a tertiary stage, where the composite creep rate increases monotonically over the steady-state value, leading to sample failure.

When the composite is subjected to a tensile stress, the tertiary creep stage can be caused by such phenomena as fiber, matrix, or interface failure, while, in compression, the tertiary stage could be caused by the four additional phenomena (brooming, bulging, kinking and buckling), all of which are characterized by a common mechanism, *i.e.*, fiber deflections away from the loading axis. Brooming and bulging, where the fiber deflections are typically rotationally symmetrical about the loading axis, exhibit out-of-loading-plane fiber deflections, while fiber deflections are typically constrained to a single plane when kinking occurs. Buckling can occur in either mode.

Brooming and bulging, which display a strong dependence on the local stress states at the regions of application of stresses, are classified as end-effect phenomena and are not examined further in the present article. When the end-effects are suppressed, buckling or kinking becomes the dominant mode of deformation and, thus, represents the bulk behavior of the material. The influence on buckling and kinking of extrinsic factors (*i.e.*, temperature and stress) and intrinsic factors (*i.e.*, fiber volume fraction and defect geometry) is examined in the following sections, and their effects on the composite creep rate are established.

A. *Model for Composite Deformation by Fiber Kinking*

In developing the model for fiber kinking, the following assumptions are made.

Table I. Experimental Parameters for the 1025 °C Compressive Creep Investigation of NiAl-W Composites

Experiment	Stress (MPa)	Aspect Ratio/ Cross Section/ Platen	$\dot{\varepsilon}_{min}$ (s^{-1})	ε_t (Pct)	ε_{total} (Pct)	Tungsten Volume Fraction (Pct)	Tertiary Type
1	80	2/C/R	$1.6 \cdot 10^{-6}$	3.0	19.0	6	bulging
2	80	2/C/F	$1.3 \cdot 10^{-6}$	3.5	8.5	7	buckling
3	80	4/S/R	$1.5 \cdot 10^{-7}$	10.5	13.5	8	bulging
4	80	2/C/F	$4.9 \cdot 10^{-7}$	5.0	11.0	8	brooming
5	80	2/C/F	$2.0 \cdot 10^{-7}$	3.5	18.0	9	brooming
6	80	2/S/F	$4.6 \cdot 10^{-7}$	7.0	18.0	10	brooming
7	80	2/S/F	$3.0 \cdot 10^{-7}$	8.0	15.0	10	brooming
8	120	2/S/F	$2.1 \cdot 10^{-5}$	5.5	10.3	11	mixed*
9	120	4/S/R	$8.0 \cdot 10^{-7}$	6.0	13.5	12	brooming
10	120	2/S/R	$9.6 \cdot 10^{-7}$	4.0	2.5	12	—
11	120	2/S/R	$1.8 \cdot 10^{-5}$	10.0	14.0	12	brooming
12	120	2/S/R	$3.5 \cdot 10^{-7}$	5.5	19.0	13	bulging
13	120	2/S/R	$7.6 \cdot 10^{-7}$	2.0	2.4	14	—
14	120	4/S/R	$6.4 \cdot 10^{-7}$	3.5	14.0	15	kinking
15	120	4/S/R	$3.5 \cdot 10^{-7}$	3.0	14.0	16	kinking

S = square cross section, C = circular cross section, F = flat platens, R = recessed platens, $\dot{\varepsilon}_{min}$ = minimum creep rate, ε_t = critical strain for onset of tertiary creep, ε_{total} = total creep strain accumulated, and * a combination of fiber buckling and partial kinking was observed.

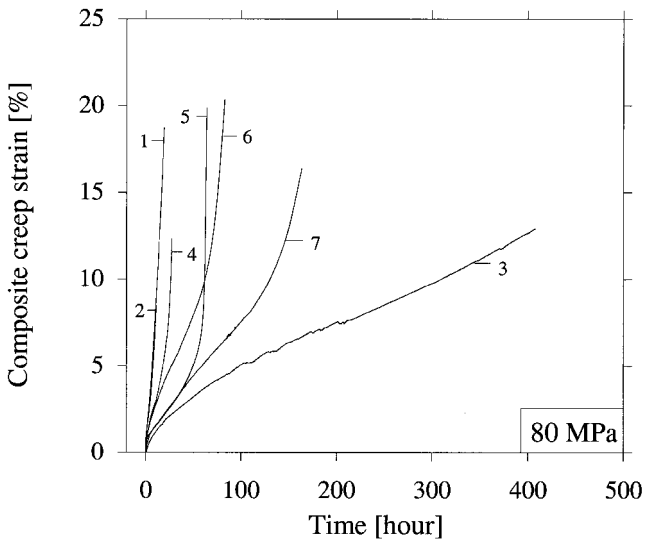

Fig. 1—Creep curves for NiAl-W composites tested at 1025 °C and 80 MPa (Table I).

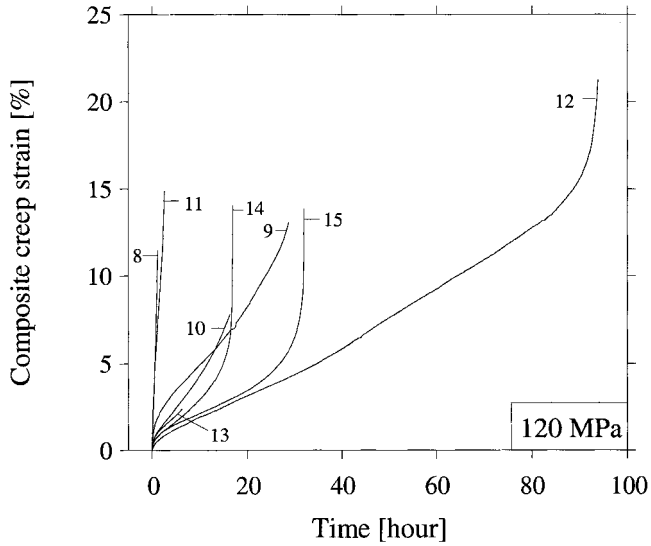

Fig. 2—Creep curves for NiAl-W composites tested at 1025 °C and 120 MPa (Table I).

(1) Processing of long-fiber composites results in local imperfections in fiber alignment (Figure 4(a)).
(2) As kinking involves fiber rotations/deflections that are typically constrained to a single plane, the problem is treated under plane-stress conditions (*i.e.*, out-of-loading-plane fiber deflections are not considered).
(3) Upon application of a far-field composite stress, the kinked region, being transversely isotropic, is loaded in a direction that does not contain a symmetry plane, and a net plastic shear strain is developed in the local volume element (Figure 4(b)).
(4) Since the matrix deforms by creep, for which the material volume is conserved, the plastic shear strain developed in the local-volume element is transmitted across the entire width of the material, causing all other fibers to rotate from their originally straight geometries, thus creating a kink band (Figure 4(b)). The kink fraction is assumed to be constant during composite-creep deformation. That this is a reasonable assumption is illustrated through a parametric analysis in a later section (Figure 10(a)), where it is shown that the overall composite-creep behavior is relatively insensitive to the kink fraction.
(5) The bending stiffness of the creeping fibers is assumed to be low, and, hence, rotations in the originally misoriented fiber translate fully and immediately to other straight fibers.
(6) The composite creep rate in the direction of the applied stress is obtained as the sum of the strain rates in the kink band and in the unkinked portions of the material, weighted according to their corresponding lengths (Figure 4(c)).
(7) At the late stages of the tertiary stage, when the kink band is fully developed, the composite is expected to

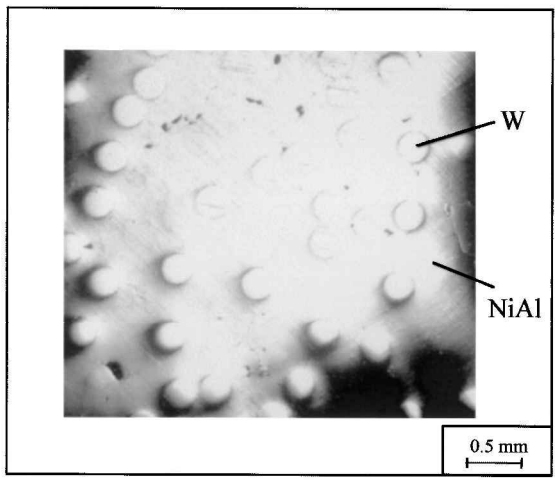

(*a*)

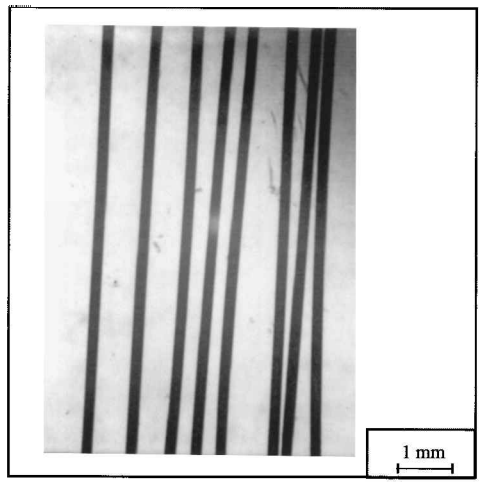

(*b*)

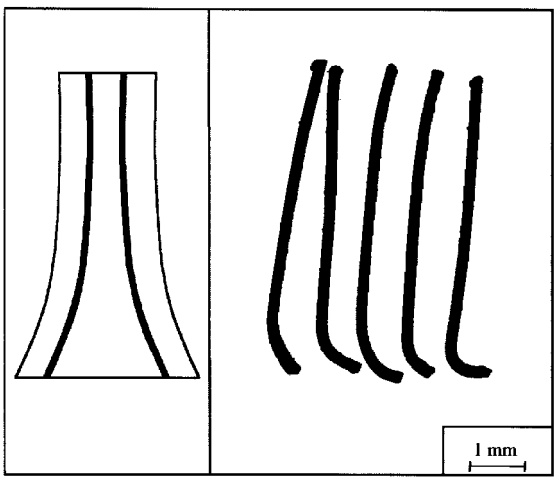

(*c*)

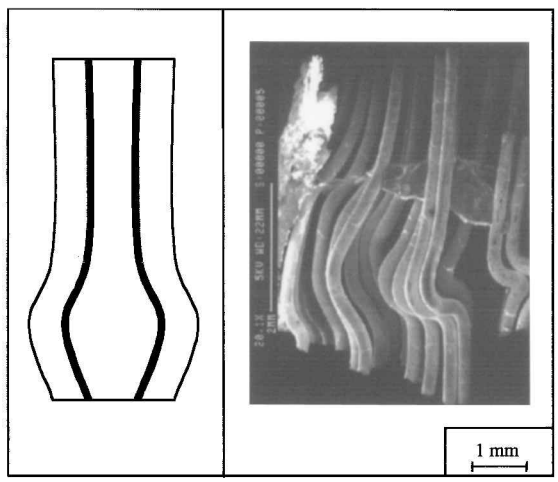

(*d*)

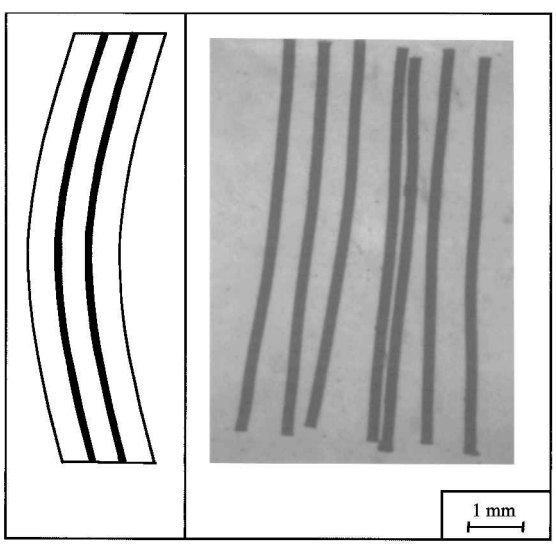

(*e*)

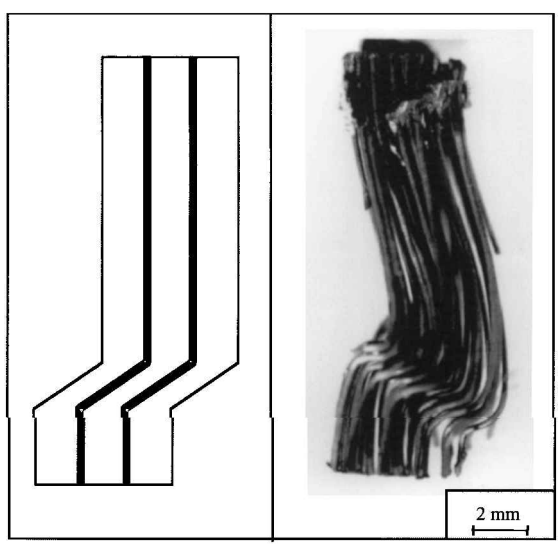

(*f*)

Fig. 3—(*a*) Cross section of the NiAl-W composite 15 showing tungsten fibers embedded in the NiAl matrix as well as tungsten fibers extracted from (*b*) untested composite and from creep tested composites 6, 12, 2, and 15, respectively, exhibiting (*c*) brooming, (*d*) bulging, (*e*) buckling, and (*f*) kinking behavior.

experience bending moments, and the global stress state is no longer expected to be purely uniaxial. The bending moments are expected to increase the creep rate of the composite. This model, by neglecting the additional

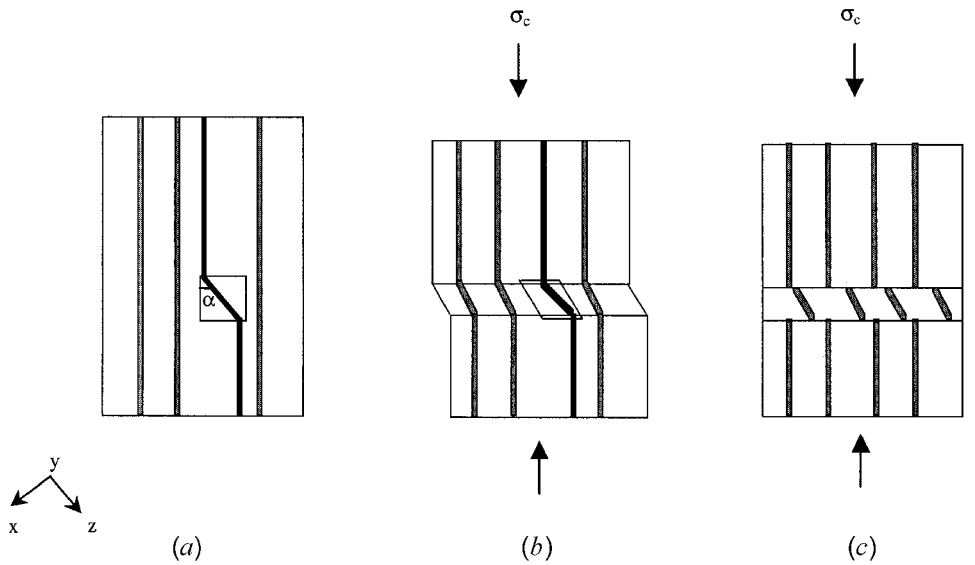

Fig. 4—Schematic of fiber kinking model for tertiary creep: (*a*) initial fiber configuration, (*b*) development of a kink band after deformation, and (*c*) trilayered composite approximating case (b) used in the model.

creep-rate contribution from the bending moments, presents a lower bound for the composite creep rate.

(8) Processing-induced residual stresses are assumed to decay quickly during the sample preheating stage and are ignored.

Following assumption 6, the creep rate of a composite with a kink band of length L_k and a straight unkinked segment of length L_u is given as

$$\dot{\varepsilon}_c = l_k\,\dot{\varepsilon}_k + (1 - l_k)\dot{\varepsilon}_u \qquad [1]$$

where the kink fraction is defined as $l_k = L_k/(L_k + L_u)$ and where $\dot{\varepsilon}_k$ and $\dot{\varepsilon}_u$ represent strain rates in the kinked and unkinked regions of the material, respectively, in the direction of the applied compressive stress. The strain-rate contribution from the straight segment can be modeled exactly as[7]

$$\sigma_c = v_f\left(\frac{\dot{\varepsilon}_u}{K_f}\right)^{1/n_f} + v_m\left(\frac{\dot{\varepsilon}_u}{K_m}\right)^{1/n_m} \qquad [2]$$

where σ_c is the applied composite stress; v_f and v_m are the fiber and matrix volume fraction, respectively; n_m and n_f are the matrix and fiber stress exponents, respectively; and K_m and K_f are the matrix and fiber creep constants in the creep power law:

$$\dot{\varepsilon} = K\sigma^n \qquad [3]$$

At 1025 °C, the values for n and K are, respectively, 5.6 and $6.37 \cdot 10^{-14}$ $MPa^{-5.6}$ s^{-1} for NiAl and 6.8 and $3.48 \cdot 10^{-26}$ $MPa^{-6.8}$ s^{-1} for tungsten (Figure 5).[16]

Equation [2] describes a relationship between stress and strain rate that does not conform to a power law when a wide stress range is considered. However, within a limited range of stresses, the composite creep rate can be accurately captured by a power law (Figure 5):

$$\dot{\varepsilon}_u = K_c\sigma_c^{n_c} \qquad [4]$$

where n_c and K_c are the stress-exponent and creep constants respectively, for the composite.

The strain-rate contribution from the kink band is obtained

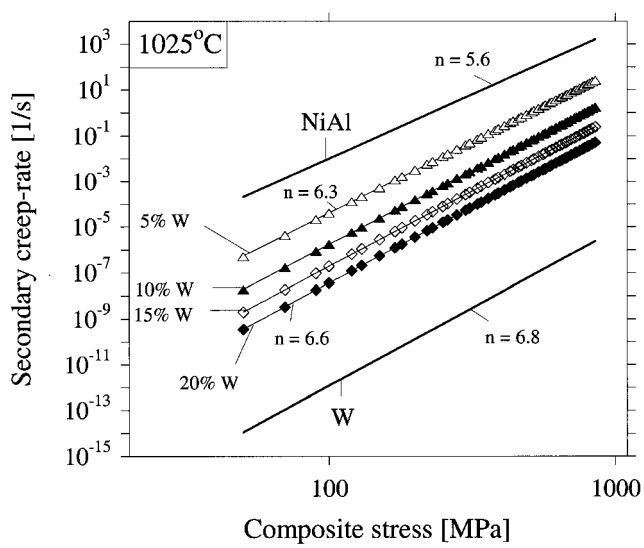

Fig. 5—Calculated NiAl-W composite secondary creep rates (Eq. [2]) at 1025 °C (symbols) showing best-fit power-law lines (Eq. [3]) with respective stress exponents for different volume fractions of tungsten and within the stress range 50 to 850 MPa.

following Johnson's approach.[26] In its original form, Johnson's model was developed to describe the overall *tensile* creep response of long-fiber composites with fibers that were misoriented at a certain angle to the loading axis. Hence, issues of kinking or buckling, which are primarily *compressive* creep responses, were not addressed. However, in the current approach, by recognizing that the kinked region in a composite subjected to a compressive stress is analogous to a compressively stressed composite with fibers misoriented to the loading axis, the results of Johnson's model can be extended to describe the creep behavior of the kink band as well.

The applied uniaxial composite stress state σ_c is transposed to an equivalent three-component multiaxial stress state consisting of a compressive stress parallel to the fiber

axis (σ_{zz}), a compressive stress normal to the fiber (σ_{xx}), and a shear stress in a plane parallel to the fibers (σ_{xz}):

$$\sigma_{zz} = \sigma_c \cos^2 \alpha \quad [5]$$

$$\sigma_{xx} = \sigma_c \sin^2 \alpha \quad [6]$$

$$\sigma_{xz} = \sigma_c \cos \alpha \sin \alpha \quad [7]$$

where α is the fiber orientation with respect to the loading direction.

The corresponding strain-rate components in the plane of deformation are[26]

$$\dot{\varepsilon}_{zz} = U^{\frac{n_c-1}{2}} \sigma_c^{n_c} \left(-\frac{1}{2} \lambda \sin^2 \alpha + \lambda \cos^2 \alpha \right) \quad [8]$$

$$\dot{\varepsilon}_{xx} = U^{\frac{n_c-1}{2}} \sigma_c^{n_c} \left(\mu \sin^2 \alpha - \frac{1}{2} \lambda \cos^2 \alpha \right) \quad [9]$$

$$\dot{\varepsilon}_{xz} = \frac{1}{2} U^{\frac{n_c-1}{2}} \sigma_c^{n_c} (\nu \sin \alpha \cos \alpha) \quad [10]$$

where U is given as

$$U = \lfloor \lambda \cos^4 \alpha + (\lambda - \nu) \sin^2 \alpha \cos^2 \alpha + \mu \sin^4 \alpha \rfloor \quad [11]$$

and λ, ν, and μ are material constants.

The strain rate in the loading direction is given by the transformation

$$\dot{\varepsilon}_\alpha = \dot{\varepsilon}_{zz} \cos^2 \alpha + \dot{\varepsilon}_{xx} \sin^2 \alpha + 2\dot{\varepsilon}_{xz} \sin \alpha \cos \alpha \quad [12]$$

Using Eqs. [8] through [11] in Eq. [12] gives[26]

$$\dot{\varepsilon}_\alpha = U^{\left(\frac{n_c+1}{2}\right)} \sigma_c^{n_c} \quad [13]$$

For a particular temperature and fiber volume fraction, the independent parameters λ, ν, and μ (all in the units of $(\text{MPa}^{-n_c}\ \text{s}^{-1})^{[2/(n_c+1)]}$ are obtained from Eq. [13] by using three different creep tests on long-fiber composites with fibers aligned at three different angles to the loading direction α, *i.e.*, α_1, α_2, and α_3, the details of which are discussed in Appendix A.

Thus, using Eqs. [13], [11], [4], and [2] in Eq. [1], the isothermal compressive creep rate of a composite with a certain initial kink fraction and initial fiber misorientation in the direction of the applied composite stress is obtained as

$$\dot{\varepsilon}_c = l_k (\lambda \cos^4 \alpha + (\lambda - \nu) \sin^2 \alpha \cos^2 \alpha + \mu \sin^4 \alpha)^{\left(\frac{n_c+1}{2}\right)} \sigma_c^{n_c} + (1 - l_k) K_c \sigma_c^{n_c} \quad [14]$$

where the parameters K_c and n_c and λ, μ, and ν, respectively, describe the creep behavior of the unkinked (straight) region and the kink band of the composite. All these five parameters implicitly depend on the volume fraction of fibers in the composite.

With deformation, the fibers rotate away from the loading axis and α increases. This increases the creep-rate contribution from the kink band (Eq. [13]) and, thus, results in an increase in the composite creep rate. As the creep-rate equations are implicit in nature, a numerical approach is adopted to solve for the composite creep rates in an incremental manner over a sequence of finite time steps, assuming the creep rates to remain constant for each time step. Appendix B describes the procedure that was adopted to account for the changing fiber angle during creep deformation.

1. *Application of the fiber-kinking model to a NiAl-W composite*

The model is illustrated in a parametric study, for the NiAl-W composite system at 1025 °C. The variation with fiber volume fraction and applied composite stress of the material parameters λ, μ (calculated using the lower-bound limit in Eq. [A4]), and ν (obtained using $\alpha = 89$ deg) is examined in Figures 6(a) through (c). As predicted by Eq. [A3], λ is independent of stress but decreases with increasing fiber volume fraction, while μ and ν are dependent on stress and, in general, decrease with increasing stress for a particular fiber volume fraction. When the upper-bound limit in Eq. [A4] is chosen for the computation of μ, the functional dependence with stress of μ and, correspondingly, ν remains unchanged, while the actual magnitudes of μ and ν at any given stress are marginally higher than those obtained by using the lower-bound limit (Figures 7(a) and (b)). The parameter λ is independent of $\dot{\varepsilon}_{90}$ and, hence, does not depend on the choice of the upper-or lower-limit bound in the calculation of μ in Eq. [A4].

In Figure 8, the variation of the kink-band creep rate as function of the kink angle α at 1025 °C, under a compressive stress of 120 MPa, is examined for a range of volume fractions of tungsten from 5 to 20 pct. The model demonstrates that (1) kink-band creep rates exhibit a weak dependence on changes in α for low values of α; (2) kink-band creep rates increase rapidly with small changes in α, at intermediate values of α; and (3) at higher values of α (*i.e.*, $\alpha > 60$ deg), kink-band creep rates converge to values very close to the matrix strain rate. It is evident that the upper-bound calculations, that assume $\dot{\varepsilon}_c^{ub} = \dot{\varepsilon}_m$ (represented by dotted lines in Figure 8), display the same qualitative and virtually the same quantitative functional dependence as the lower-bound calculations, that assume $\dot{\varepsilon}_c^{lb} = v_f \dot{\varepsilon}_f + (1 - v_f)\dot{\varepsilon}_m$ (represented by solid lines in Figure 8).

The tertiary kink model is applied to a composite with an initial kink angle of 2 deg and an initial kink fraction of 1/10. Figure 9 shows that the composite creep rate exhibits three stages with increasing strain. In the first stage, the composite creep rate remains almost constant. This region is associated with small rotations of the fibers in the kink band. In the second stage, the composite creep rate increases rapidly with composite strain. This is associated with the rapid acceleration in fiber rotations in the kink band. In the third stage, the composite creep rate converges to a new steady state ($\approx l_k \dot{\varepsilon}_{90}$).

The main results from this analysis are as follows.

(1) The critical threshold strain, defined by the completion of stage 1 and onset of stage 2, varies inversely with the volume fraction of the composite. This implies that composites with higher volume fractions of reinforcements are more susceptible to the onset of compressive-creep instability in the form of kinking. This is because the higher-volume-fraction composites exhibit greater anisotropy in creep strengths, and, thus, fiber rotations cause a relatively higher increase in creep rates.
(2) The new steady state is also reached at the smallest composite strain by the composite with the highest volume fraction of fibers.

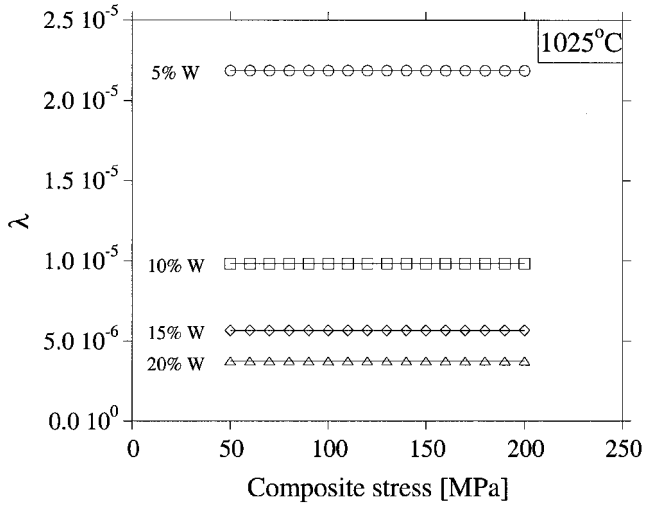

(*a*)

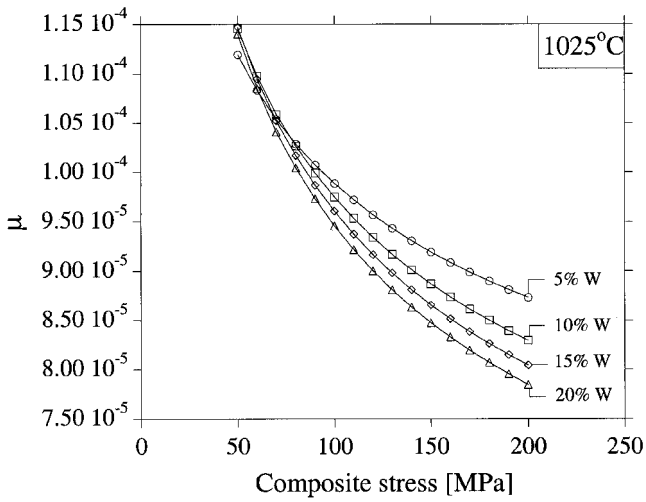

(*b*)

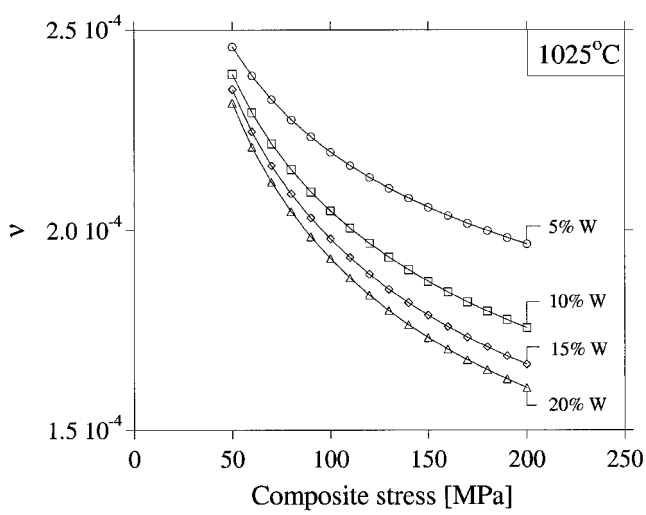

(*c*)

Fig. 6—Variation of the kink-band creep parameters (*a*) λ, (*b*) μ, and (*c*) ν (Eq. [13]) with composite stress for different tungsten fiber volume fractions for NiAl-W composites at 1025 °C. (The lower bound in Eq. [A4] is used for this simulation.)

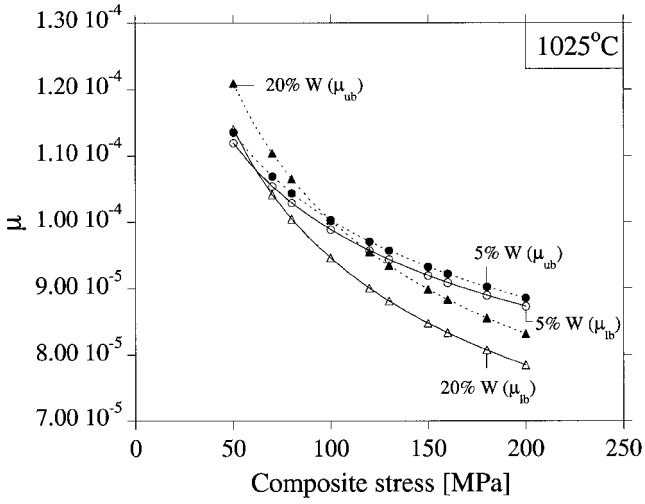

(*a*)

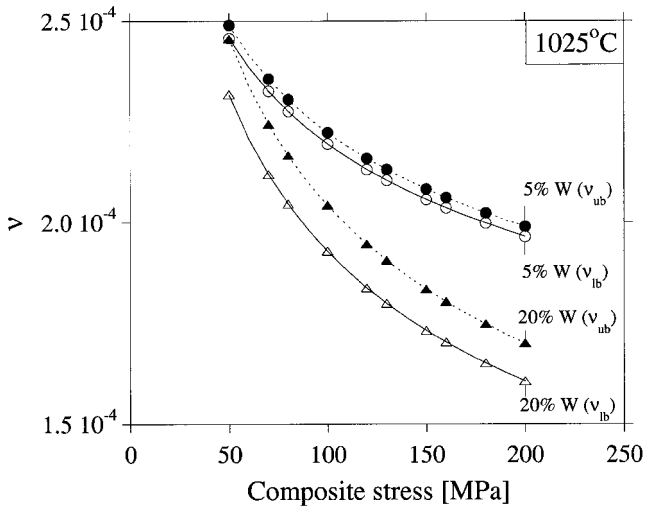

(*b*)

Fig. 7—Variation of the kink-band creep parameters (*a*) μ and (*b*) ν (Eq. [13]) with composite stress for different tungsten fiber volume fractions for NiAl-W composites at 1025 °C. (The lower bound in Eq. [A4] is represented by the solid line and open symbols, while the upper bound is represented by dotted lines and filled symbols.)

(3) While a new steady state is predicted by this model to occur in the third stage, it is unlikely that such a stage might ever be reached in reality, as the problem moves to the domain of large deformations, with the local strains in the kink band being very inhomogeneous and much larger than the composite strain. From a practical viewpoint, it is of little interest to model this stage, as the composite would be deemed to have failed soon after the onset of the tertiary stage, where very large accumulations in creep strain occur over a short period of time.

(4) The upper-bound calculations (represented by dotted lines in Figure 9) follow the trends predicted by the lower-bound calculations (represented by solid lines in Figure 9). As expected, the upper-bound model predicts the onset of the second stage to occur at marginally lower composite strains and the composite creep rate to converge to a new steady state that is marginally higher than that predicted by the lower-bound model.

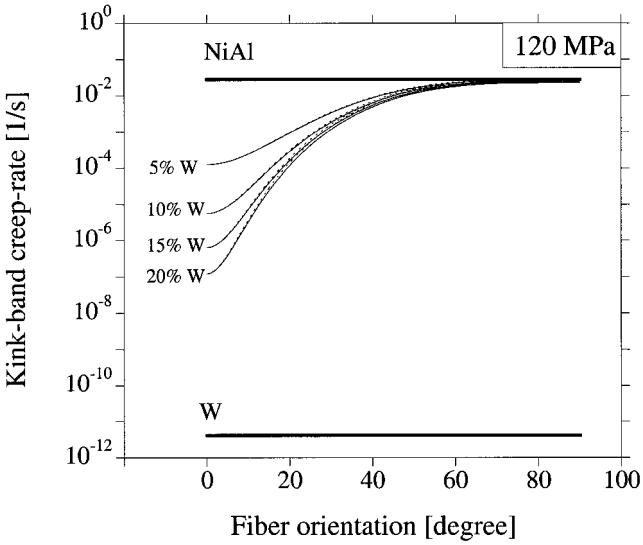

Fig. 8—Calculated variation of the kink-band creep rate (Eq. [13]) with fiber orientation with respect to the loading direction at 1025 °C, 120 MPa, and for varying volume fractions of tungsten. (Solid lines represent lower bound limit, while dotted lines represent the upper bound limit in Eq. [A4].)

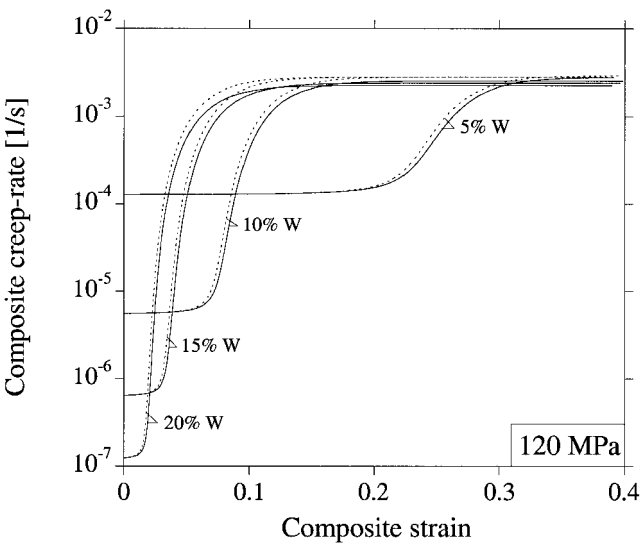

Fig. 9—Predictions of tertiary kink-band model (Eqs. [1], [2], and [13]) for NiAl-W composites with an initial kink angle of 2 deg and an initial kink fraction of 1/10 showing composite creep rate as a function of composite strain under an applied composite stress of 120 MPa. (Solid lines represent lower bound limit, while dotted lines represent the upper bound limit in Eq. [A4].)

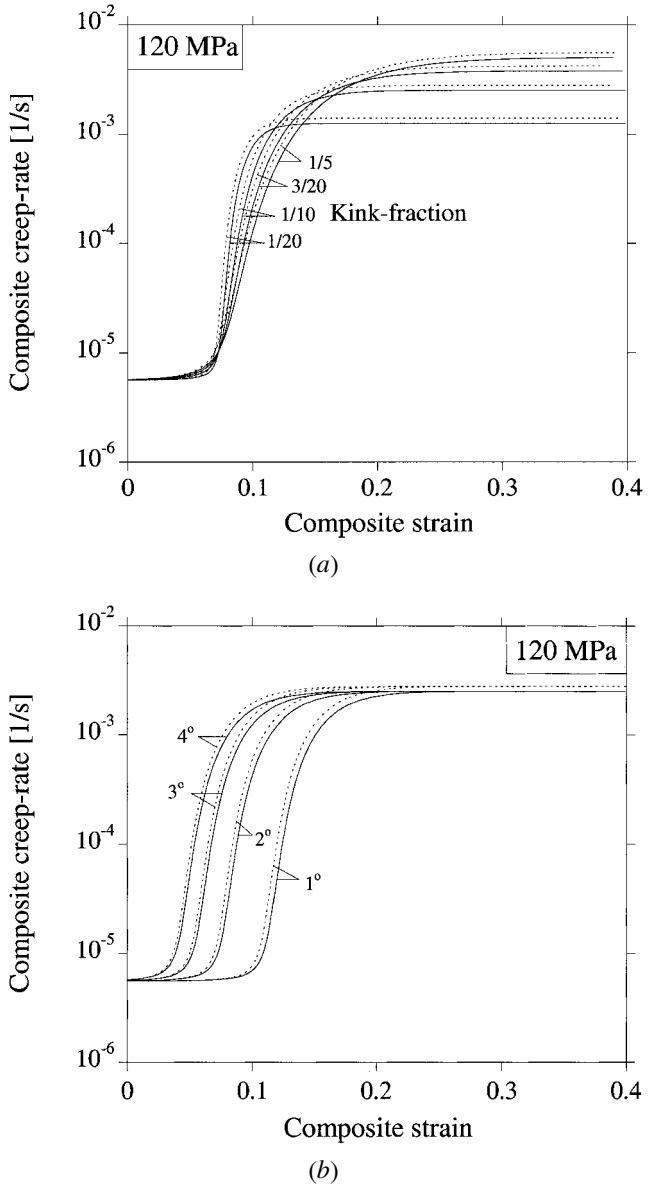

Fig. 10—Predictions of the tertiary kink-band model (Eqs. [1], [2], and [13]) for a NiAl-10 vol pct W composite: (*a*) with a constant initial kink angle of 2 deg but with different initial kink fractions; and (*b*) with a constant initial kink fraction of 1/10 but with different initial kink angles, each figure showing composite creep rates as functions of composite strain under an applied composite stress of 120 MPa. (Solid lines represent lower bound limit, while dotted lines represent the upper bound limit in Eq. [A4].)

Figure 10(a) examines the effect on the composite tertiary behavior due to changes in initial kink fraction from 1/20 to 1/5 at a constant initial kink angle of 2 deg at 1025 °C, 120 MPa, and 10 pct W. This figure shows that the critical strain threshold for the onset of stage 2 remains almost invariant with changes in the initial kink fractions. However, the steady states in stage 3 are different for the different composites. The composite with the highest initial kink fraction converges to the highest creep rate. This is because the strain-rate contribution from the kink band in stage 3 is about $l_k \dot{\varepsilon}_{90}$.

Figure 10(b) illustrates the effect on the composite tertiary behavior due to changes in initial kink angles from 1 to 4 deg at a constant initial kink fraction of 1/10 at 1025 °C, 120 MPa, and 10 pct W. This figure shows that the critical strain threshold for the onset of stage 2 varies inversely with the initial kink angle. This is because, for a composite with a given volume fraction of reinforcement, there exists a critical threshold for the kink angle α above which the material moves into the tertiary regime. If the initial kink angle is larger, then the material reaches this threshold value at a lower value of composite strain. Also, all composites converge to the same steady-state creep rate at the end of stage 2. This is because the kink fraction is the same for all the composites. From Figures 10(a) and (b), it is evident that the upper- and lower-bound models predict qualitatively and

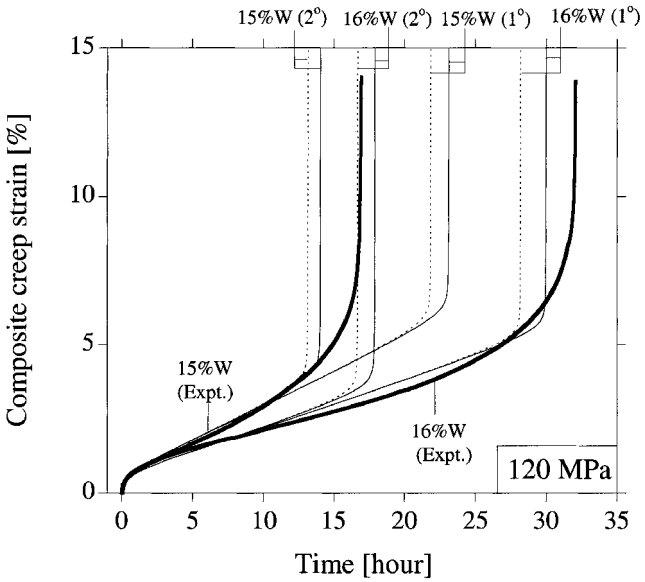

Fig. 11—Creep curves as predicted by the tertiary kink-band model (Eqs. [1], [2], and [13]) and as measured in experiments 14 (15 vol pct W) and 15 (16 vol pct W). The composite primary creep predictions are from Ref. 15. (Solid lines represent lower bound limit, while dotted lines represent the upper bound limit in Eq. [A4].)

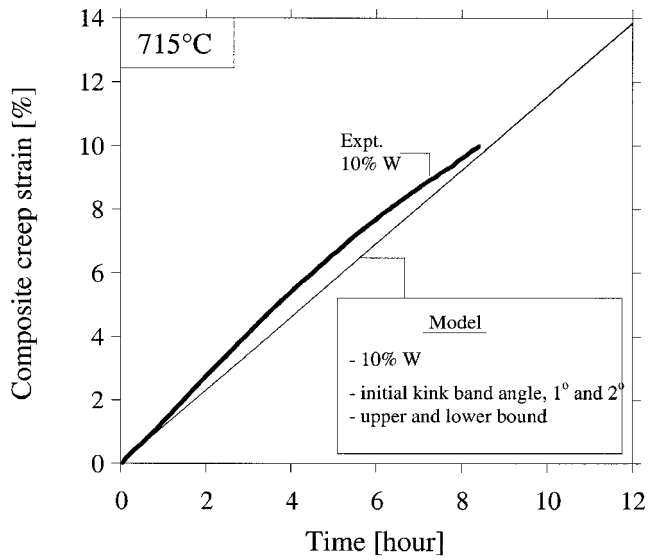

Fig. 12—Creep curve predicted by the tertiary kink-band model (Eqs. [1], [2], and [13]) and as measured in the 715 °C experiment on a NiAl-10 vol pct W composite (experiment 20 in Ref. 16) at 300 MPa.

quantitatively similar results for the composite tertiary behavior.

2. *Experimental verification of the fiber-kinking model*

In compression-creep experiments conducted on NiAl composites reinforced with 5 to 20 vol pct W, brooming and bulging were the most common modes of deformation (Table I). In two cases (14 and 15, Figure 2), the NiAl-W composite samples with tungsten volume fractions of 15 and 16 pct and a sample aspect ratio of 4, subjected to an initial stress of 120 MPa at 1025 °C, exhibited pure kinking. Figure 11 compares the measured creep curves with theoretical predictions, assuming an initial kink angle of 1 or 2 deg and using the experimentally determined kink fraction of 1/10 (Figure 3(f)). The primary creep behavior of the matrix and the fiber are incorporated in the model predictions as well.[15] In general, there is fair agreement between theory and experiments. The experimentally observed creep behavior for the 15 pct W composite lies in between the model predictions that assume an initial kink angle of 1 and 2 deg, while, for the 16 pct W composite, the experimentally observed behavior is closer to the model prediction that assumes an initial kink angle of 1 deg.

The differences between the predicted and observed creep behavior (Figure 11) can be explained as arising from the model assumptions that local shear strains in regions where fibers are misaligned are transmitted fully and immediately to all other fibers, and, thus, the kink band sweeps through the entire width of the sample. In reality, the kink bands are not expected to traverse the entire width, especially at the early stages. Hence, it takes a longer time for the kink band to fully develop and for the fibers in the kink band to rotate past the critical threshold angles. Additionally, the model simulations assumed constant stress conditions, while the experiments were performed under constant initial load conditions. With creep deformation, the composite stress is expected to decrease and, thus, would reduce the composite creep rate and increase the time for onset of the tertiary stage.

Compression-creep experiments were also performed on the NiAl-W system at 715 °C at 300 MPa and are reported in Reference 16. For these experiments, no tertiary behavior was observed. The secondary creep rate observed in experiment 20 in Reference 16 with 10 vol pct W exhibited the best correlation to the model predictions based on the rule of mixtures (Eq. [2]) and, hence, is selected for comparison with the tertiary model discussed in this article. As the NiAl-W composite samples tested at 715 °C were fabricated by the same technique that was used to obtain the samples for the 1025 °C experiments, the initial fiber-defect geometry in the 715 °C experiments is expected to be identical to that which was present in the 1025 °C experiments. Hence, using the 715 °C matrix and fiber creep parameters (Eq. [3]) that were experimentally determined and reported in Reference 16, initial kink angles of 1 or 2 deg, and an initial kink fraction of 1/10, the fiber-kinking model is derived for both the upper- and lower-bound conditions (Eq. [A4] and Figure 12). The fiber-kinking model does not predict a tertiary behavior within the first 40 pct (shown up to 14 pct in Figure 12) of composite-creep strain, consistent with experimental observation. Because both the NiAl matrix and the W fiber are considerably more creep resistant at 715 °C than at 1025 °C, the kink-band creep rates at 715 °C are much lower than those observed at 1025 °C. Hence, the onset of stage 2 (as seen in Figure 9 for 1025 °C) is expected to occur when the composite strains are much greater than at 1025 °C. (At this stage, the experiment can no longer be considered to be a creep experiment, where the typical strains accumulated are on the order of a few percents). The marginal decrease in the composite-creep secondary creep rate observed in the experiment (Figure 12) is attributed to the decrease in composite stress with deformation.

Thus, the presence and absence of a tertiary stage in the NiAl-W composite-creep behavior, respectively, at 1025 °C and 715 °C can be considered in a self-consistent manner using the fiber-kinking model.

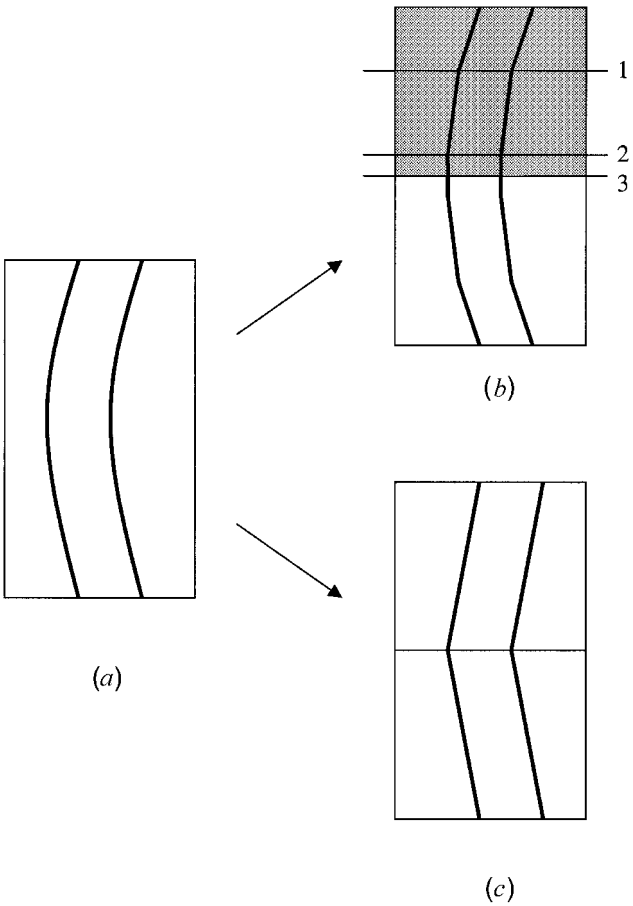

Fig. 13—Schematic of fiber buckling model: (*a*) composite with curved, buckled fibers; (*b*) multilayerd composite approximating case (a); and (*c*) bilayered composite used in the model.

B. *Model for composite deformation by fiber buckling*

For NiAl-W composites produced by reactive infiltration,[16] there could be fiber waviness (illustrated schematically in Figure 13(a)) due to (1) nonuniform layup of tungsten fibers in the porous nickel-wire preform prior to infiltration; (2) inhomogeneous infiltration forces that are generated in the nickel preform upon infiltration; and (3) elasto-plastic curvature induced by thermal-mismatch stresses developed upon cooling the composite from 1638 °C to room temperature during processing and upon heating to test temperatures.

A composite with buckled fibers can be treated, in the most general case, as a multilayered composite (Figure 13(b)), or, in the simplest case, as a two-layered composite, each layer with fibers that are straight but misoriented with the loading direction (Figure 13(c)). For the purpose of illustration, the latter case is investigated, where the composite is modeled as two large kink-bands symmetric about the midsection of the sample and spanning its entire height. Hence, all of the assumptions presented earlier for the kink-band model apply to this buckling model as well, and the composite creep rate is given by Eq. [13].

The tungsten fibers extracted from a typical NiAl-W composite by dissolving the matrix exhibit curvatures that can be well approximated by a two-layered composite model (Figure 3(b)). The angles of misorientation range from <1 to about 2 deg, with a median misorientation of 1 deg. The procedures adopted in measuring the misorientation angles are discussed in detail in Reference 14. As expected, the composite creep rate increases with deformation (Figure 14) as a result of fiber rotations within the kink band. The calculated creep curves (Figure 15) indicate the presence of a critical strain above which deformation is very rapid and which varies inversely with the volume fraction of fibers in the composite, as in Figure 9. As the fiber volume fraction increases, the difference in the critical time for the onset of

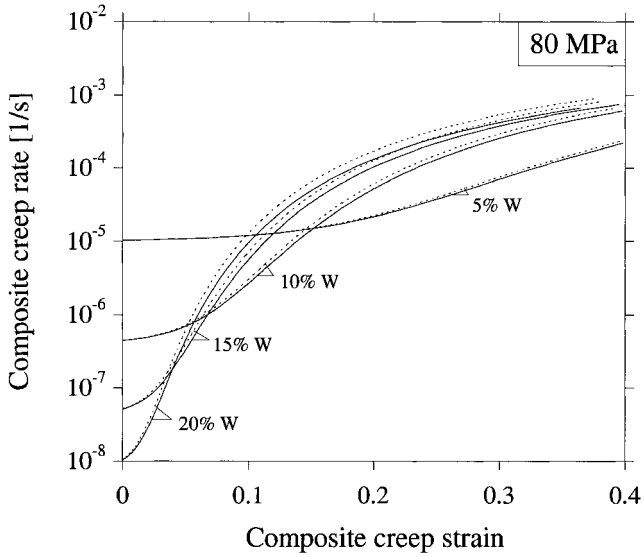

Fig. 14—Predictions of the buckling model (Eq. [13]) for a NiAl-W composite with varying volume fractions of tungsten (for the case when the initial kink angle is 2 deg) at 1025 °C and an applied stress of 80 MPa showing composite creep rate as a function of composite creep strain. (Solid lines represent lower bound limit, while dotted lines represent the upper bound limit in Eq. [A4].)

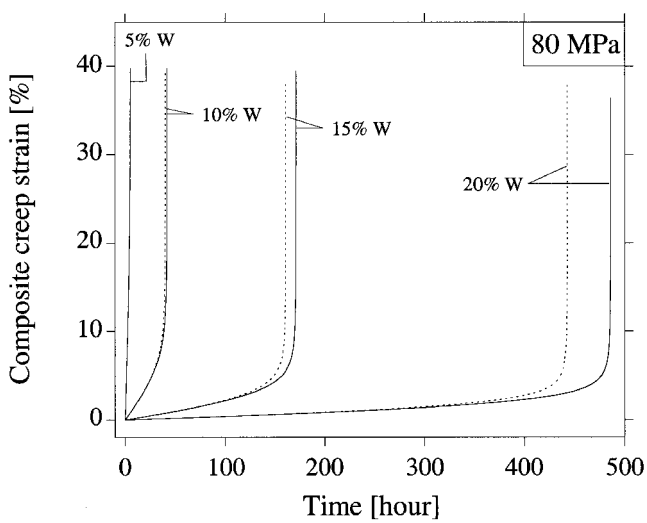

Fig. 15—Predictions of the fiber buckling model for a NiAl-W composite with varying volume fractions of tungsten (for the case when the initial kink angle is 2 deg) at 1025 °C and an applied stress of 80 MPa showing composite creep strain as a function of time. (The model predictions do not incorporate the primary creep of the NiAl matrix or the tungsten fibers. Solid lines represent lower bound limit, while dotted lines represent the upper bound limit in Eq. [A4].)

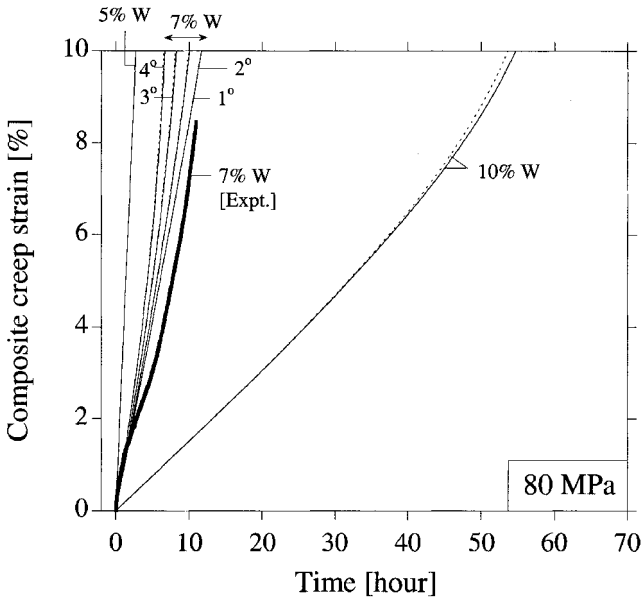

Fig. 16—Creep curves as predicted by the buckling model for different volume fractions and for different initial fiber orientations for 7 pct W, compared to experiment 2. (The model predictions do not incorporate the primary creep of the NiAl matrix or the tungsten fibers. Solid lines represent lower bound limit, while dotted lines represent the upper bound limit in Eq. [A4]. The 5 and 10 pct W composite curves were obtained using an initial fiber misorientation angle of 1 deg.)

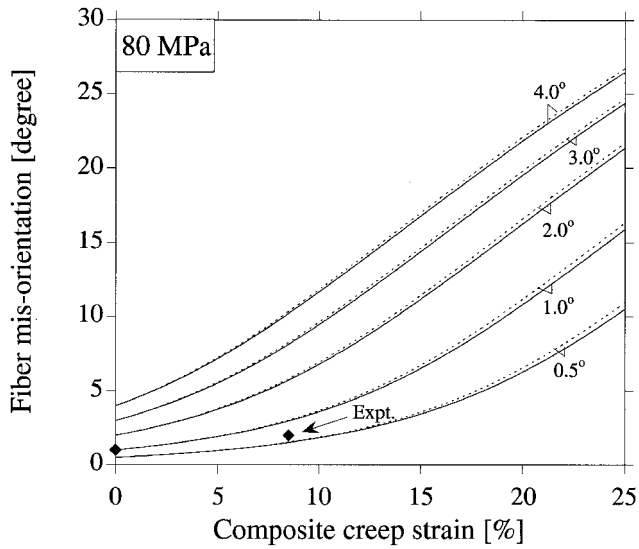

Fig. 17—Predictions of the buckling model (Eq. [13]) for a NiAl-7 pct W composite at 1025 °C and 80 MPa, showing evolution of fiber misorientation as a function of composite creep strain for different initial fiber orientation and compared to experiment 2. (Solid lines represent lower bound limit, while dotted lines represent the upper bound limit in Eq. [A4].)

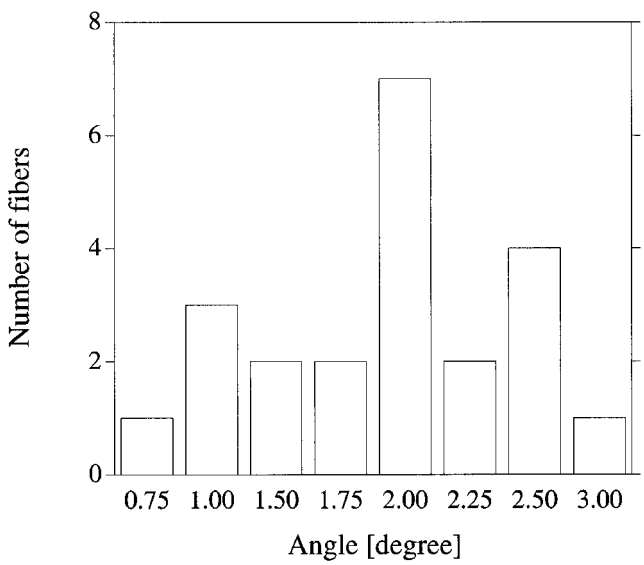

Fig. 18—Analysis of fiber orientations in experiment 2, 1025 °C and 80 MPa after 8.5 pct creep strain.

the tertiary stage, predicted by the upper-bound (dotted lines in Figure 15), and the lower-bound models (solid lines in Figure 15) becomes more significant.

In Figure 16, the buckling-model predictions (Eq. [13]) are compared to experiment 2, which is the only case where buckling of the fibers was observed (Figure 3(e)). Using the initial fiber misorientation of 1 deg, reasonable agreement is found between the experiment and model predictions. The sensitivity of the composite strains to the initial misorientation of fibers is examined in Figure 16 for fiber misorientations from 1 to 4 deg. This figure shows that the sensitivity increases with increasing strain levels, as indicated by the divergent creep curves.

Finally, the evolution of fiber rotation with deformation is illustrated in Figure 17 for a NiAl-7 vol pct W composite at 80 MPa. This figure shows that both the upper-bound model and the lower-bound model predict that the fibers with an initial misalignment of 1 deg will rotate to attain a new orientation of 2 deg at a strain of 8.5 pct. The experimental observation of the deformed fibers also indicates the fiber rotations to be approximately 2 deg (Figure 18), thus demonstrating reasonable agreement of the model predictions with the experimental results.

As discussed in the earlier section, the 715 °C simulations (at 300 MPa) for identical initial fiber geometries indicate that the tertiary stage does not occur in the experimentally measured creep-strain range, in agreement with experimental observations.[16]

Finally, the limitations of the buckling model are addressed as follows. First, the model approximates a composite with curved fibers as a bilayered composite with fibers that are straight but misaligned (Figure 13(c)) and computes an upper bound to the steady-state strain rates. A more accurate but computation-intensive analysis could be done following the multilayered construct (Figure 13(b)), by applying the same procedure to each layer and computing the average strain rate of each layer weighted by their corresponding length scales to obtain the composite creep rate. Second, the model assumes that fiber deformation occurs in one plane. However, out-of-plane deformations have been observed, so that a three-dimensional formulation would be required for a more accurate analysis. Third, the initial fiber imperfection is taken to be symmetric about the midsection of the sample, so that fiber deflections evolve in a symmetric manner with deformation; asymmetry in the initial fiber configuration needs to be addressed. Fourth, local matrix stresses generated by deflecting fibers[27] and their effects on the composite creep are assumed to be negligible. Fifth, some of the tungsten fibers have been observed to kink

locally, while others buckled globally (experiment 8). Such complex mixed modes cannot be modeled with the present formulation.

V. CONCLUSIONS

The high-temperature uniaxial compression-creep behavior of unidirectionally reinforced continuous-fiber composites was investigated using NiAl-W as a model system for the case where both the NiAl matrix and the tungsten fibers underwent plastic deformation by creep. While, in general, these composites exhibited classical three-stage creep behavior with distinct primary, secondary, and tertiary stages, this article focused on their tertiary creep behavior.

1. Microstructurally, tertiary creep was characterized by four fiber-deformation mechanisms (*i.e.*, brooming, bulging, buckling, and kinking), all of which involved fiber deflections away from the loading axis. Buckling and kinking were typically characterized by in-plane fiber deflections and represented the bulk behavior of the composite. Brooming and bulging were typically characterized by axi-symmetric fiber deflections and displayed a strong dependence on the local stress states at the regions of application of the compressive stresses and were classified as end-effect phenomena.
2. A simple kink-band model was developed that predicted (1) the critical strain for the onset of the tertiary stage to be most sensitive to the initial kink angles and relatively insensitive to the initial kink-band heights, and (2) the critical strain to vary inversely with the volume fraction of fiber in the composites. For the two experiments where fiber kinking was observed, reasonable agreement with the model predictions was obtained.
3. By extension of the kink-band model, the effects of fiber buckling were also examined. For the experiment where fiber buckling was observed, reasonable agreement with the model predictions was obtained.
4. At 715 °C, the fiber kinking/buckling models do not predict a tertiary stage in the compressive-creep behavior of NiAl-W composites, consistent with experimental observations.

ACKNOWLEDGMENTS

This work was supported by the National Science Foundation through Grant No. MSS 9201843, monitored by Dr. B. McDonald. The authors also acknowledge the financial support of the Department of Materials Science and Engineering, MIT, in the form of teaching assistantships BrTAV and the AMAX career development chair BrDCD. One of the authors (TAV) also acknowledges Professor S. Suresh for funding in the form of a postdoctoral position at MIT during which time this article was completed.

APPENDIX A

For determining the three material constants (λ, ν, and μ) that describe the kink-band deformation, three creep tests on composites with fibers aligned at three angles to the loading direction, *i.e.*, α_1, α_2, and α_3 are required.

For the first test, we chose $\alpha_1 = 0$ deg. The composite creep rate is then predicted exactly by Eq. [2], for composites with strong fiber/matrix interfaces.[7] It has also been demonstrated (Ref. [A1]) that the zone of dislocation interaction with the fibers is on the order of about 1 μm. Hence, in composites with large fiber diameters (>100 μm), the effects of dislocation interaction at the fiber-matrix interface are expected to be small and can be ignored. As the experiments in this investigation have been performed on the NiAl-W composite system, where the NiAl/W interface is strong and the fiber diameter is large (250 μm), the choice of Eq. [2] as representing the composite creep rate for $\alpha_1 = 0$ deg. is justified.

For the second test, we chose $\alpha_2 = 90$ deg. Here, two limiting cases can be identified: (1) an upper bound, or an overestimate, where the composite creep rate $\dot{\varepsilon}_c^{ub}$ can be set equal to the matrix creep rate,

$$\dot{\varepsilon}_c^{ub} = \dot{\varepsilon}_m \qquad [A1]$$

and (2) a lower bound, or an underestimate, where the composite creep rate $\dot{\varepsilon}_c^{lb}$ can be taken to be equal to the average of that of the matrix and the fiber, weighted by their respective volume fractions as

$$\dot{\varepsilon}_c^{lb} = v_f \dot{\varepsilon}_f + (1 - v_f)\dot{\varepsilon}_m \qquad [A2]$$

For fiber composites with strong interfaces, even though the fibers are oriented at 90 deg to the loading axis, some creep strengthening is expected due to load transfer from the matrix to the fiber, and, thus, the composite creep rate is expected to be lower than that of the matrix. On the other hand, the degree of strengthening is expected to be lower than that offered by a lamellar (plate-like) composite of the same volume fraction, as the matrix flow around the lamellae is strictly restricted in this iso-stress/lower-bound model (Eq. [A2]). Thus, the true creep rate of the composite where the fibers are orientated at 90 deg to the loading axis is expected to be lower than that of the matrix (Eq. [A1]) but higher than that predicted by Eq. [A2]. However, for composites where the matrix creep rate dominates over that of the fiber and the fiber volume fractions are low, the results predicted by the upper-bound model do not vary significantly from those predicted by the lower-bound model.

For the third test, we chose $\alpha_3 = 89$ deg and set the composite creep rate at $\alpha_3 = 89$ deg as equal to that for $\alpha_2 = 90$ deg. That this is a reasonable approximation is borne out by an inspection of the results of the creep experiments of Miles and McLean (Ref. [A2]) in the (Co,Cr)-$(Co,Cr)_7C_3$ system at 825 °C with different fiber orientations, where, for large values of α (>60 deg), the observed composite creep rate converged to the composite creep rate corresponding to $\alpha = 90$ deg. While the parameters λ and μ can be determined from the 0- and 90- deg experiments, ν can be rigorously obtained by choosing the 40- or 60- deg experiments. If, however, we ignore the real (40 or 60 deg) experiments and choose a virtual (89 deg) experiment and set the composite creep rate at $\alpha_3 = 89$ deg as equal to that for $\alpha_2 = 90$ deg, we note that, qualitatively and quantitatively, the functional dependence of the kink-band creep behavior with fiber orientation to the loading direction does not change significantly (Figure A1). Thus, for the purpose of illustration and without loss of generality, we set the composite creep rate at $\alpha_3 = 89$ deg as equal to that for $\alpha_2 = 90$ deg. In summary, while the mathematics of Johnson's model require three different creep tests, we invoke the physical argument that the composite behavior is virtually invariant with changes in α at large values of α, and, thus, in effect, we reduce the model to a two-parameter model.

By applying the first test (setting $\alpha = 0$ deg in Eq. [11]

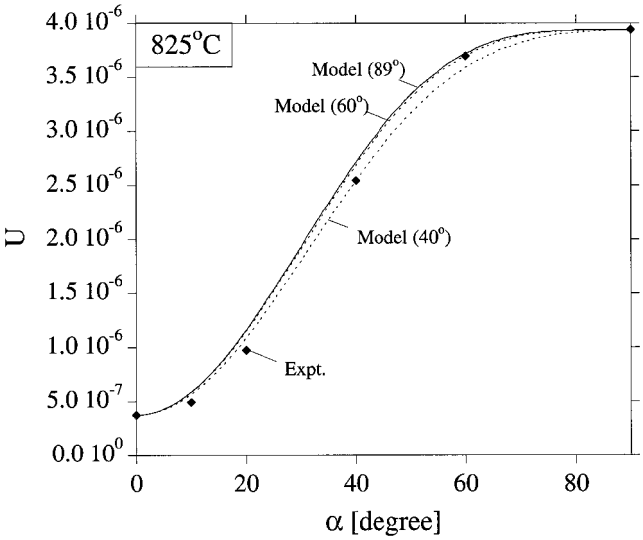

Fig. A1—Comparison of experimental results of Miles and McLean (Fig. A2) with theoretical values of $U(\alpha)$ calculated from Eq. [11] using 40 and 60-deg experiments and the proposed methodology with $\alpha = 89$ deg.

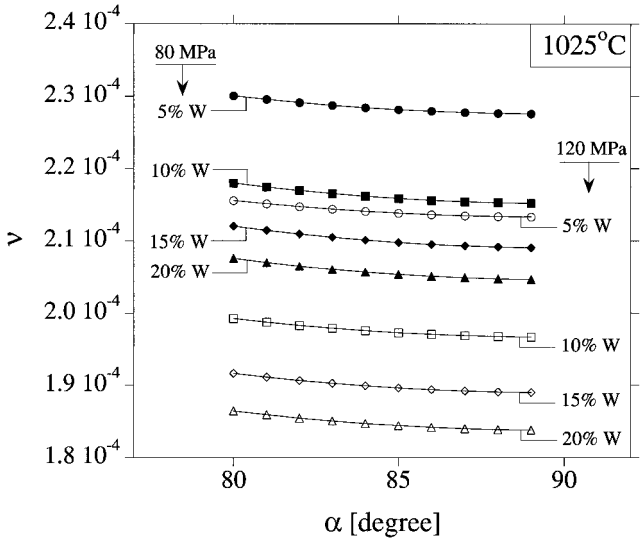

Fig. A2—Variation of ν with choice of α between 80 and 89 deg for the determination of the third boundary condition, for different tungsten fiber volume fractions at composite stresses of 80 and 120 MPa for NiAl-W composites at 1025 °C.

and using Eqs. [4] and [11] in Eq. [13], the parameter λ is obtained as

$$\lambda = K_c^{\left(\frac{2}{n_c+1}\right)} \qquad [A3]$$

By applying the second test (setting $\alpha = 90$ deg in Eq. [11] and using Eqs. [A1] and [A2] in Eq. [13]), the parameter μ is obtained as

$$\mu = \left(\frac{\dot{\varepsilon}_{90}}{\sigma_c^{n_c}}\right)^{\left(\frac{2}{n_c+1}\right)} \qquad [A4]$$

where $\dot{\varepsilon}_{90} = \dot{\varepsilon}_c^{ub}$ or $\dot{\varepsilon}_{90} = \dot{\varepsilon}_c^{lb}$, depending on the choice of the two limiting cases discussed previously.

Using Eq. [11] in Eq. [13], the constant ν is obtained in the general form as

$$\nu = \lambda + \left(\frac{\left(\frac{\dot{\varepsilon}_\alpha}{\sigma_c^{n_c}}\right)^{\left(\frac{2}{n_c+1}\right)} - \lambda \cos^4 \alpha - \mu \sin^4 \alpha}{\sin^2 \alpha \cos^2 \alpha} \right) \qquad [A5]$$

Setting $\alpha = 89$ deg in Eqs. [11], [13], and [A5], using Eq. [A4], and invoking the physical argument that $\dot{\varepsilon}_{89} \approx \dot{\varepsilon}_{90}$, the particular solution for ν is obtained as

$$\nu = \lambda + \left(\frac{\mu - \lambda \cos^4 89 \text{ deg} - \mu \sin^4 89 \text{ deg}}{\sin^2 89 \text{ deg} \cos^2 89 \text{ deg}} \right) \qquad [A6]$$

(In the limit $\alpha \to 90$ deg Eq. [A6] gives $\nu \to \lambda + 2\mu$).

The sensitivity of ν to the choice of α between 80 and 89 deg (with the corresponding $\dot{\varepsilon}_{(80 \text{ to } 89)} \approx \dot{\varepsilon}_{90}$) is examined in Figure A2, for composites with fiber volume fractions between 5 and 20 pct at 80 and 120 MPa. It can be concluded from this analysis that ν does not vary significantly with the choice of α (for values of α between 80 and 89 deg).

REFERENCES (APPENDIX)

A1. S. Goto and M. McLean: *Acta Mater.*, 1991, vol. 39, pp. 153-64.
A2. D.E. Miles and M. McLean: *J. Met. Sci.*, 1977, vol. 11, pp. 563-70.

APPENDIX B

Upon the application of a compressive stress to a kink band that has fibers misoriented at an angle of α with respect to the loading axis, the fibers tend to rotate away from the loading axis. The procedure that has been used to track this fiber rotation is discussed as follows. Let OA (Figure B1) and α_0 represent the initial length and initial misorientation of the fibers in the kink band. Assuming the creep rate of the kink band in the loading direction (given by Eq. [13]) to be constant in an infinitely small time interval, the kink-band displacement in the loading direction is computed as

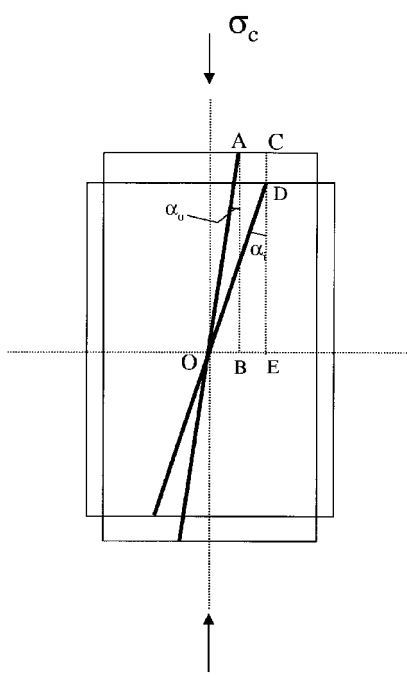

Fig. B1—Schematic illustrating the method for determining the fiber orientation with creep deformation in the kink band.

the length CD. In the same time interval, using Eq. [8] and also assuming the creep rate of the kink band in the fiber direction to be constant, the new length of the fiber OC is computed. (Due to compressive creep, the fiber length OC is shorter than the initial length OA). The angle ODE, thus, yields the new orientation, α_i, of the fiber. This procedure is subsequently repeated to track the fiber rotations with creep deformation of the kink band.

REFERENCES

1. K.K. Chawla: *Composite Materials*, Springer-Verlag, New York, NY, 1987.
2. B.W. Rosen: *Fiber Composite Materials*, ASM, Metals Park, OH, 1965, pp. 37-75.
3. A.S. Argon: in *Treatise on Materials Science and Technology*, H. Herman, ed., Academic Press, New York, NY, 1972, pp. 79-114.
4. B. Budiansky and N.A. Fleck: *J. Mech. Phys. Solids*, 1993, vol. 41, pp. 183-211.
5. C.R. Schultheisz and A.M. Waas: *Prog. Aerospace Sci.*, 1996, vol. 32, pp. 1-42.
6. A.M. Waas and C.R. Schultheisz: *Prog. Aerospace Sci.*, 1996, vol. 32, pp. 43-78.
7. M. McLean: *Mechanical Behavior of In-Situ Composites*, The Metals Society, London, 1983, pp. 207-56.
8. W.S. Slaughter, N.A. Fleck, and B. Budiansky: *Trans. ASME- J. Eng. Mater. Technol.*, 1993, vol. 115, pp. 308-13.
9. R.R. Bowman: in *Intermetallic Matrix Composites II*, D.B. Miracle, D.L. Anton, and J.A. Graves, eds., Materials Research Society, Pittsburgh, PA, 1992, pp. 145-55.
10. D. Proulx and F. Durant: in *Failure Modes in Composites II*, J.N. Fleck and R.L. Mehan, eds., TMS-AIME, New York, NY, 1974, pp. 188-96.
11. D.E. Alman and N.S. Stoloff: *Scripta Mater.*, 1993, vol. 30, pp. 203-08.
12. C.H. Weber, K.T. Kim, F.E. Heredia, and A.G. Evans: *Mater. Sci. Eng.*, 1995, vol. 196, pp. 25-31.
13. D.H. Nguyen and A.A. Ogale: *J. Thermal Comp. Matter.*, 1991, vol.4, pp.83-99.
14. T.A. Venkatesh: Ph.D. Thesis, Massachusetts Institute of Technology, Cambridge, MA, 1998.
15. T.A. Venkatesh and D.C. Dunand: *Acta Mater.*, 1999, vol. 47, pp. 4275-82.
16. T.A. Venkatesh and D.C. Dunand: *Metall. Trans.*, 2000, vol. 31, pp. 781-92.
17. D.B. Miracle: *Acta Mater.*, 1993, vol. 41, pp. 649-84.
18. R.D. Noebe, R.R. Bowman, and M.V. Nathal: *Int. Mater. Rev.*, 1993, vol. 38, pp. 193-232.
19. D.M. Dimiduk, D.B. Miracle, and C.H. Ward: *Mater. Sci. Techn.*, 1992, vol. 8, pp. 367-75.
20. N.S. Stoloff: *Metall. Trans.*, 1993, vol. 24A, pp. 561-67.
21. S.L. Robinson and O.D. Sherby: *Acta Mater.*, 1969, vol. 17, pp. 109-25.
22. J.W. Pugh: *Proc. ASTM*, 1957, vol. 57, pp. 909-16.
23. B. Harris and E.G. Ellison: *Trans. ASM*, 1966, vol. 59, pp. 744-54.
24. A.K. Misra: Report No. CR 4171, NASA, Washington, DC, 1988.
25. C.W. SanMarchi and A. Mortensen: *Metall. Trans.*, 1998, vol. 29A, pp. 2819-28.
26. A.F. Johnson: *J. Mech. Phys. Solids*, 1977, vol. 25, pp. 117-26.
27. M.R. Piggott: *J. Mater. Sci.*, 1981, vol. 16, pp. 2837-45.